



## Passive direct formic acid microfabricated fuel cells

J. Yeom<sup>a</sup>, R.S. Jayashree<sup>b</sup>, C. Rastogi<sup>b</sup>, M.A. Shannon<sup>a</sup>, P.J.A. Kenis<sup>a,b,\*</sup>

<sup>a</sup> Department of Mechanical & Industrial Engineering, University of Illinois at Urbana-Champaign, 1206 Green Street, Urbana, IL 61801, USA

<sup>b</sup> Department of Chemical & Biomolecular Engineering, University of Illinois at Urbana-Champaign, 600 S. Mathews Avenue, Urbana, IL 61801, USA

Received 28 December 2005; received in revised form 14 February 2006; accepted 14 February 2006

### Abstract

This paper reports on microscale silicon-based direct formic acid fuel cells (Si-DFAFCs) in which the fuel and the oxidant are supplied to the electrodes in a passive manner. Passive delivery of fuel and oxidant eliminates the need for ancillary components and associated parasitic losses. In this Si-DFAFC, an aqueous solution of formic acid is in direct contact with a Pd- or Pt-based anode and a Pt-based cathode is exposed to either a forced oxygen stream or quiescent air. In the presence of a forced oxygen flow on the cathode side the cell with Pd catalyst on the anode delivers a maximum power density of about 30 mW cm<sup>-2</sup> at room temperature, limited mostly by mass transfer at the anode, while in an all-passive mode (quiescent air on the cathode side) a maximum power density of 12.3 mW cm<sup>-2</sup> is obtained, limited by oxygen transport. This all-passive Si-DFAFC is fabricated using processes that are post-CMOS compatible, and thus can be integrated directly with envisioned MEMS applications, such as small sensors and actuators.

© 2006 Elsevier B.V. All rights reserved.

**Keywords:** Micro fuel cell; Membrane electrode assembly; Formic acid; Passive fuel cell

### 1. Introduction

Many efforts are presently directed to develop micro fuel cells as power sources for a wide range of portable applications [1–26]. When integrating micro fuel cells as on-chip power sources into MEMS sensors/actuators and microchemical systems, manufacturing processes for both membrane electrode assembly (MEA) and the remaining fuel cell systems must be post-CMOS compatible. Conventional, Si-based [1–4,8,11–15,17–19,22–25] and non-conventional, polymer-based [5,6,9,10,20] microelectronic/MEMS fabrication methods have been used to obtain a wide variety of electrode designs and flow channels. Most studies, however, utilized spray-coating or painting techniques to deposit catalyst on the membranes to form the MEAs. Such methods may not be suitable for integration with MEMS fabrication processes. Alternatively, several micro fuel cells that have the catalysts layer formed using post-CMOS compatible methods: either electrodeposition on a car-

bon support [11,12,18] or sputter-deposition on a support electrode and/or membrane [5,6,8,19]. The latter sputtered or evaporated catalysts typically exhibit low performance (<1 mW cm<sup>-2</sup>) due to their inherently small surface areas. Previously, we have reported on silicon-based microfabricated membrane electrode assemblies (Si-MEAs) in which high-surface-area Pt, Pd, and Pt/Pd catalyst structures are introduced directly on a gold current collector by electrodeposition [22,23]. Those Si-MEAs produced power densities up to 35 mW cm<sup>-2</sup> when using a stream of hydrogen as the fuel with electrodeposited Pt catalyst structures [22], whereas a similar Si-MEA with Pd catalyst structures as the anode operated with 10 M formic acid produced a maximum power density of 28 mW cm<sup>-2</sup> [23].

Micro fuel cells can be operated with forced streams of different fuels, including hydrogen [1–10], methanol [11–21], and formic acid [22,26]. Hydrogen, although considered an ideal fuel from a reaction kinetics point of view, is difficult to store at high energy density, particularly at the microscale. Methanol, as a liquid fuel is easier to store, has a high energy density, and is most widely used in micro fuel cells. Multiple microfabricated *direct methanol fuel cells* (DMFCs) have been reported in which 0.5–8 M methanol fuel solutions are supplied via forced convection to an anode comprised of Pt/Ru alloy nanoparticles [11–21]. The maximum power densities of these DMFCs range

\* Corresponding author at: Department of Chemical & Biomolecular Engineering, University of Illinois at Urbana-Champaign, 600 S. Mathews Avenue, Champaign, IL 61801, USA. Tel.: +1 217 265 0523; fax: +1 217 333 5052.

E-mail address: kenis@uiuc.edu (P.J.A. Kenis).

from  $5 \mu\text{W cm}^{-2}$  to  $20 \text{mW cm}^{-2}$  at room temperature. These DMFCs, however, suffer from fuel crossover when polymer electrolytes such as Nafion are used, leading to mixed potentials on the cathode side, and thus a dramatic loss in cell performance. As an alternative, *direct formic acid fuel cells* (DFAFCs) have been reported for portable power sources, which utilize the faster kinetics, compared to methanol, of formic acid electro-oxidation at room temperature, and the lower tendency of formic acid to exhibit fuel crossover across Nafion membranes [26–29]. For example, Ha et al. recently reported mesoscale DFAFCs with a forced fuel feed producing a maximum power density of  $248 \text{mW cm}^{-2}$  [30,31]. Although the theoretical energy density of formic acid ( $1700 \text{Wh kg}^{-1}$  or  $2086 \text{Wh L}^{-1}$ ) is less than one-third of methanol ( $6100 \text{Wh kg}^{-1}$  or  $4690 \text{Wh L}^{-1}$ ), the lower rates of fuel crossover through the Nafion membrane allows for higher concentrations of formic acid than of methanol to be used. DMFCs and DFAFCs may thus actually have similar specific energies, since 4 M methanol and 10 M formic acid have similar fuel energy densities with respect to fuel volume (Table 1).

Another key challenge in downscaling fuel cell technology for portable and lab-on-a-chip applications involves miniaturization, or preferably, elimination of ancillary components such as pumps and valves for fuel and oxidant delivery. In particular, fluid pumping mechanisms do not scale down linearly, leading to higher parasitic losses and a lower overall energy density of micro fuel cell systems. To eliminate these so-called parasitic losses, a number of DMFCs and DFAFCs have been reported with *passive* means of fuel delivery and often also with an air-breathing cathode [16,32–43]. Microscale DMFCs using a passive supply of 2–5 M methanol with maximum power densities ranging from 2 to  $43 \text{mW cm}^{-2}$  have been reported [38,39,42]. A centimeter-scale passive feed DFAFC operated on 10 M formic acid was also investigated delivering a maximum power density of  $33 \text{mW cm}^{-2}$  [43]. The characteristics and performance of various all-passive DMFCs and DFAFCs are summarized in Table 1. These passive feed liquid fuel cells have the potential for a higher overall, specific energy density in a fuel cell system due to the elimination of the additional weight and volume of ancillary components that, in turn, can be replaced with additional fuel. Such passive microscale fuel cells would be promising as high energy density power sources, for example, for implementation in MEMS actuators, especially if

the fuel cells can be fabricated simultaneously using post-CMOS compatible processes.

In this paper, we report on silicon-based microfabricated direct formic acid fuel cells (Si-DFAFCs) in which fuel delivery is passive; the liquid formic acid fuel is in direct contact with the anode-side of the MEA. Analysis of the effect of the passive delivery of both formic acid and oxygen was conducted separately using various combinations of active and passive operating conditions at the respective electrodes. Polarization and power density curves of Si-DFAFCs operated with different concentrations of formic acid are presented, and the benefits and limitations of these cells are discussed.

## 2. Experimental

### 2.1. Si-MEA fabrication and assembly

Silicon-based membrane electrode assemblies (Si-MEAs) were prepared using standard MEMS fabrication processes mostly according to a procedure we reported previously [22]. In short, a 100 mm N-doped double-sided polished (100) Si wafer (Silicon Quest) was used as the supporting structure of the Si-MEA and coated with a  $1000 \text{Å}$  Au layer by dc magnetron sputtering ( $\sim 10^{-2}$  Torr of Ar background pressure). Photolithography and liftoff were then performed to create the Au current collector pattern. This pattern was subsequently spin-coated with a polyimide (PI) layer (PMDA-ODA PI2808, HD Microsystem), to provide electrical isolation between the cell halves and to serve as a spacing layer between the catalyst structures and the Nafion membrane. Next, the PI that covered the silicon not covered with Au was removed using RIE after applying a photolithographic patterned photoresist layer exactly aligned with the previously generated Au-pattern. The resulting structure forms a mask for etching of the silicon to form the  $50\text{-}\mu\text{m}$  thick grid-like Si structures with an array of  $100 \mu\text{m}^2$  holes using deep reactive ion etching (Plasma-Therm SLR 770). With the help of a shadow mask, the Au layer that covered the grid was selectively exposed with an oxygen plasma in the RIE system (Jupiter III, March Instruments), thus leaving the PI spacer layer on the Au-covered silicon around the grid untouched. Pt or Pd catalyst structures were electrodeposited to form a single catalyst-covered Si-electrode with a geometrical

Table 1  
Summary of the performance of *all-passive* (passive delivery of fuel, air-breathing, and room temperature) fuel cells available in the literature as well as the Si-DFAFC of this work

| Reference           | MEA: support and electrolyte | Anode catalyst             | Geometrical electrode area [ $\text{cm}^2$ ] | Maximum power density (MPD) [ $\text{mW cm}^{-2}$ ] | Voltage at MPD [V] | Open cell potential (OCP) [V] | Optimal [fuel] and net energy density [ $\text{Wh L}^{-1}$ ] |
|---------------------|------------------------------|----------------------------|--|---|--------------------|-------------------------------|--|
| Chang et al. [33]   | Carbon paper, co-PTFS        | PtRu nanoparticles         | 2  | 10  | 0.30               | 0.65                          | 5 M $\text{CH}_3\text{OH}$ 976                               |
| Han and Park [34]   | Carbon paper, Nafion 115     | Electroless PtRu/C         | 9  | 4   | 0.25               | 0.72                          | 2 M $\text{CH}_3\text{OH}$ 390                               |
| Shimizu et al. [38] | Carbon paper, Nafion 112     | PtRu/C nanoparticles       | 35   | 11  | 0.30               | 0.55                          | 4 M $\text{CH}_3\text{OH}$ 781                               |
| Kim et al. [39]     | Carbon paper, Nafion 115     | PtRu nanoparticles         | 6  | 40  | 0.30               | 0.78                          | 5 M $\text{CH}_3\text{OH}$ 976                               |
| Liu et al. [42]     | Carbon paper, Nafion 115     | PtRu nanoparticles         | 4  | 20  | 0.18               | 0.50                          | 5 M $\text{CH}_3\text{OH}$ 976                               |
| Ha et al. [43]      | Carbon paper, Nafion 117     | PtRu nanoparticles         | 1  | 33  | 0.25               | 0.65                          | 10 M $\text{HCOOH}$ 782                                      |
| This work           | Patterned Si, Au, Nafion 112 | Electrodeposited Pt and Pd | 0.44   | 12.3  | 0.30               | 0.60                          | 10 M $\text{HCOOH}$ 782                                      |

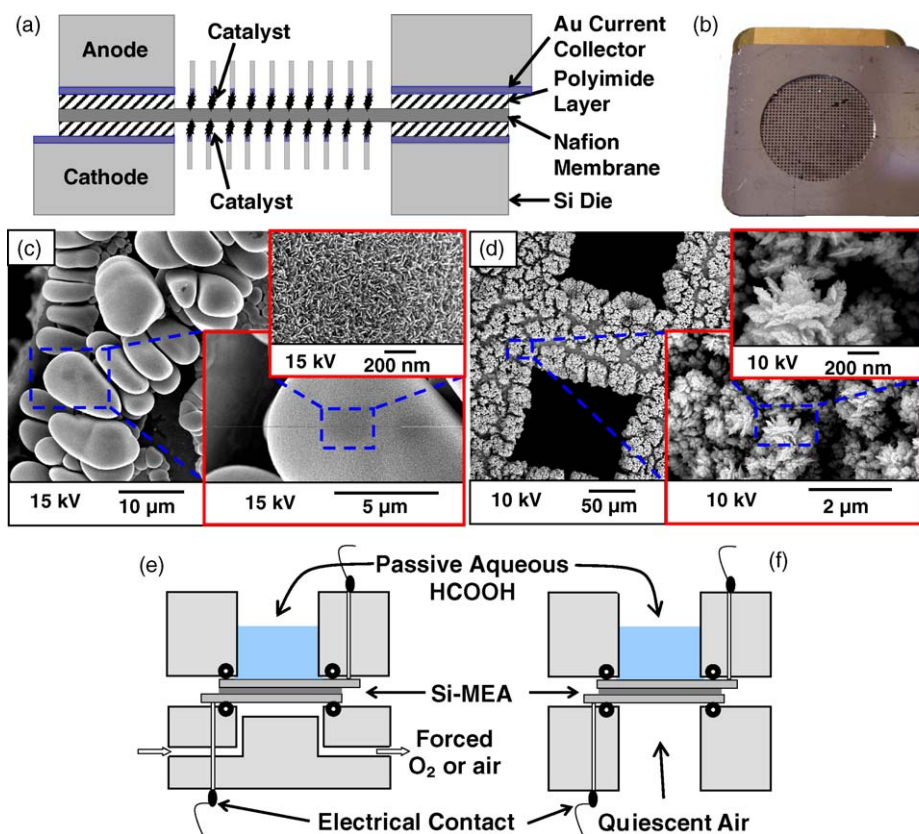


Fig. 1. (a) Schematic and (b) optical micrograph of the 18 mm  $\times$  18 mm silicon-based membrane electrode assembly (Si-MEA) used in this study [22]. (c and d) SEM images of electrodeposited Pd and Pt catalyst structures, respectively; and schematic of the test setup used to measure the fuel cell performance of the Si-DFAFCs operated with passive fuel delivery on the anode side and active oxygen/air delivery (e) or passive air delivery (f) on the cathode side.

surface area of 0.44 cm<sup>2</sup> (see below). A Nafion-112 membrane (Fuel Cell Scientific, Stoneham, MA) was sandwiched between two Si-electrodes and bonded using a hot press (EV-420 bonder, 120 °C,  $\sim$ 200 N cm<sup>-2</sup>) to yield a Si-MEA as shown in Fig. 1a and b.

## 2.2. Catalyst structure preparation

Two different anode catalyst structures, electrodeposited Pt (loading 2.5 mg cm<sup>-2</sup>) and Pd (4.0 mg cm<sup>-2</sup>), were used, while an electrodeposited Pt catalyst structure (2.5 mg cm<sup>-2</sup>) was used as the cathode in all experiments reported here. SEM images of these electrodeposited Pd and Pt catalyst structures reveal their high surface areas (Fig. 1c and d). We reported a detailed description of the procedures to deposit these Pt and Pd catalyst structures on Si-electrodes as well as their electrochemical characteristics (e.g. surface areas) earlier [23].

## 2.3. Si-DFAFC testing

To obtain a Si-DFAFC, each Si-MEA with different anode catalyst structure (Pt or Pd) was mounted on a custom-built glass-filled Teflon test fixture that can accommodate delivery of fuel and oxidant (Fig. 1e and f). Different concentrations of aqueous formic acid (ACS grade 96%, Acros) were delivered

as the fuel in a passive form by placing 2 ml of each solution directly on the anode side of the Si-MEA. We studied the performance of the Si-DFAFCs under different cathode conditions: (a) a 10 sccm stream of oxygen; (b) a 10 or 50 sccm stream of air; (c) quiescent air. Experiments (a) and (b) utilized the configuration shown in Fig. 1e, while experiment (c) was performed with the configuration shown in Fig. 1f. Since it is our purpose to eliminate ancillary components, including heaters, we conducted all fuel cell tests at room temperature. Data points of the polarization curves were recorded using a potentiostat (Autolab PGSTAT 30) by applying a constant cell potential and measuring the steady-state current after waiting for 1–3 min. The error in each point of the polarization curves is estimated to be  $\pm$ 5%.

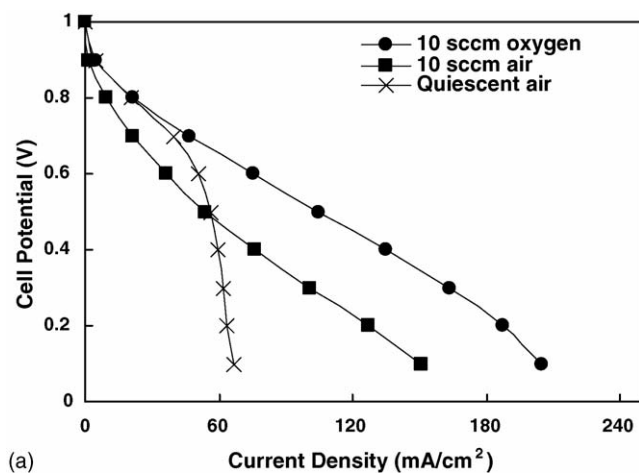
## 3. Results and discussion

In an effort to reduce parasitic losses we studied Si-DFAFCs with passive fuel and oxidant delivery: formic acid solutions of different concentrations in direct contact with the anode side of the Si-MEA and the cathode side exposed to quiescent air.

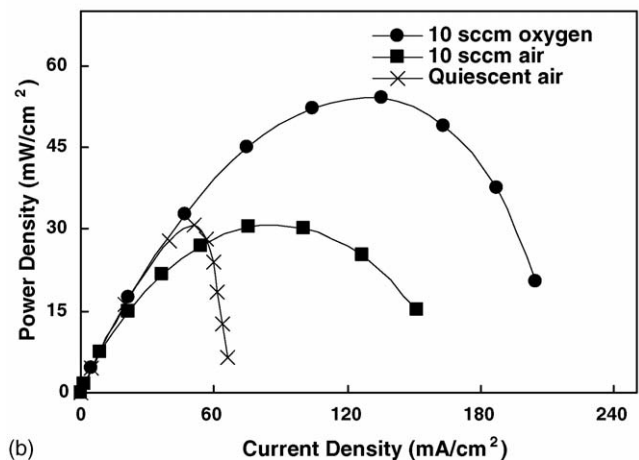
### 3.1. Cathode performance characterization

First we studied Si-DFAFCs with electrodeposited Pt catalyst structures as the anode and the cathode at room temperature

using 10 sccm of hydrogen as the fuel on the anode and three different operating conditions on the cathode: (i) 10 sccm of oxygen; (ii) 10 sccm of compressed air; (iii) quiescent air. The extent of the cathode overpotential and mass transport limitations can be revealed assuming that the anode kinetics of  $H_2$  on Pt catalysts is very fast. The open circuit potentials (OCPs) of 1 V as measured for all three conditions indicate that any anode limitation is very small (see Fig. 2a). An abrupt drop in the potential in the high current density regime in Fig. 2a clearly demonstrates the oxygen transport limitation on the cathode side for the Si-DFAFC operated with quiescent air. The better performance of the Si-DFAFC operated with forced oxygen, compared to the one operated with forced air, can be attributed to a higher driving force to replenish the depleted boundary layer on the cathode. A maximum power density of  $54 \text{ mW cm}^{-2}$  at 0.4 V was obtained for the hydrogen–oxygen case (see Fig. 2b), a 50% increase compared to our previous study [22]. This improvement in cell performance can be attributed to optimization of the thickness ( $\sim 3.5 \mu\text{m}$ ) of the polyimide spacing layer that ensures intimate contact between the catalyst structures on the Si-grid and the Nafion membrane.



(a)



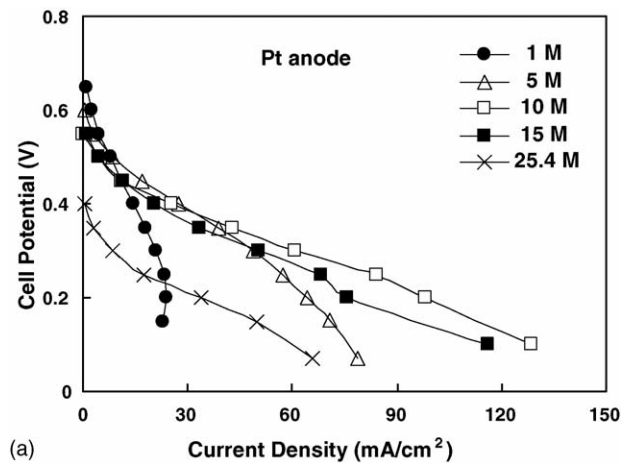
(b)

Fig. 2. Polarization (a) and power density (b) curves of a Si-DFAFC operating at room temperature with a  $H_2$  supply of 10 sccm on the anode side and three different ways of oxygen air supply on the cathode.

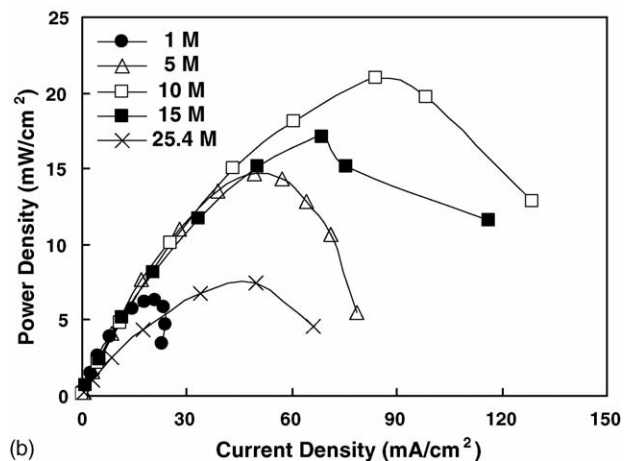
### 3.2. Pt anode performance characterization

Next, we characterized the anode performance of these Si-DFAFCs with Pt catalyst structures, while providing a forced stream (10 sccm) of oxygen on the cathode side to suppress any performance-limiting factors on the cathode side. Fig. 3 shows polarization and power density curves for Si-DFAFCs operated using different concentrations of formic acid (1–25.4 M) as the fuel. A maximum OCP of 0.66 V is obtained for 1 M formic acid. The gradual decrease in the OCP with increasing formic acid concentration is the result of an increase in formic acid crossover through the Nafion 112 membrane, a trend also observed in both actively pumped DFAFCs [26] and passive air-breathing DFAFCs [43].

Insufficient mass transport of fuel is the prevailing performance-limiting factor when low formic acid concentrations (i.e. 1–5 M) are used while the decrease of the power density at higher formic acid concentrations ( $>10 \text{ M}$ ) can be attributed to partial dehydration of the Nafion membrane [26]. Interestingly, the maximum power density measured here was significantly higher compared to our previous study:  $\sim 21 \text{ mW cm}^{-2}$  here versus  $\sim 3 \text{ mW cm}^{-2}$  previously [23]. The



(a)



(b)

Fig. 3. Polarization (a) and power density (b) curves of a Si-DFAFC operating at room temperature with quiescent aqueous  $HCOOH$  solutions of different concentrations (1–25.4 M) on the anode (pure Pt) and a 10 sccm stream of  $O_2$  on the cathode (pure Pt).

improved performance originates from the use of Pt catalyst structures with higher surfaces areas obtained as a result of deposition at higher potentials. The sharp drop in cell potential due to activation losses at low current densities ( $<10 \text{ mA cm}^{-2}$ ) is in part due to inefficient electro-oxidation of formic acid on pure Pt catalyst structures as a result of CO poisoning [23,44,45].

### 3.3. Pd anode performance characterization

We repeated the same experiment with a Si-DFAFC with electrodeposited Pd as opposed to Pt catalyst structures on the anode side, resulting in the polarization and power density curves shown in Fig. 4. Now higher maximum power densities of 33.1 and  $30.7 \text{ mW cm}^{-2}$  are measured, when using 5 and 10 M formic acid, respectively. As before the OCPs decrease with increasing formic acid concentration, but all OCPs and cell potentials are approximately 0.2 V higher at the same current density for the cells with Pd as opposed to Pt catalyst structures at the anode. The highest maximum energy and power densities for the Si-MEAs with Pd anode are already attained when using 5 M formic acid as the fuel, whereas the maximum energy and power den-

sities for the Si-MEA with Pt anode were only reached when using 10 M formic acid. The improved performance of the Si-DFAFCs with Pd rather than Pt catalyst structures is a result of significantly lower occurrence of CO poisoning of the catalyst, consistent with previous work by us [23] and others [30,31,45].

### 3.4. All-passive Si-DFAFC characterization

Finally, we exposed the cathode side to quiescent air to study the performance of a Si-DFAFC in which both fuel and oxygen feeds are passive. Fig. 5 compares the polarization curves and power density curves of Si-DFAFCs with Pd or Pt anode catalyst structures using a passive fuel feed of 10 M formic acid at the anode and a quiescent air feed at the cathode. Maximum power densities of 12.3 and  $9.1 \text{ mW cm}^{-2}$  were obtained for the Si-DFAFC with Pd and Pt anode catalyst structures, respectively. As expected, these values are lower than the performance of the same cells operated with a forced stream of oxygen at the cathode (Figs. 3 and 4). The trend of higher OCPs and current densities of Si-DFAFCs with a Pd anode, however, is preserved in these all-passive fuel cells.

The measurements on the Si-DFAFC with a forced hydrogen feed at the anode and quiescent air at the cathode (Fig. 2a) basically set the upper limit of the maximum current densities that can be obtained with an all-passive fuel cell. Comparing that data of Fig. 2a with the data of Fig. 5, we conclude that Si-DFAFCs operated in an all-passive mode (Fig. 5) are ultimately performance limited by mass transfer of oxygen when quiescent air is used on the cathode side. Lifetime tests of the performance of the all-passive Si-DFAFC with Pd catalyst operated at 0.3 V with a 10 M formic acid solution exhibited a rapid initial decay in current within the first 3 min, followed by a slow linear decay of about 25% over 1 h. This behavior is identical to that of DFAFCs reported by Ha et al. [30], and as was the case for those DFAFCs, we were able to recover the original performance of our all-passive Si-DFAFC by applying an anodic potential of 1 V versus DHE. The Si-DFAFCs studied here exhibit similar perfor-

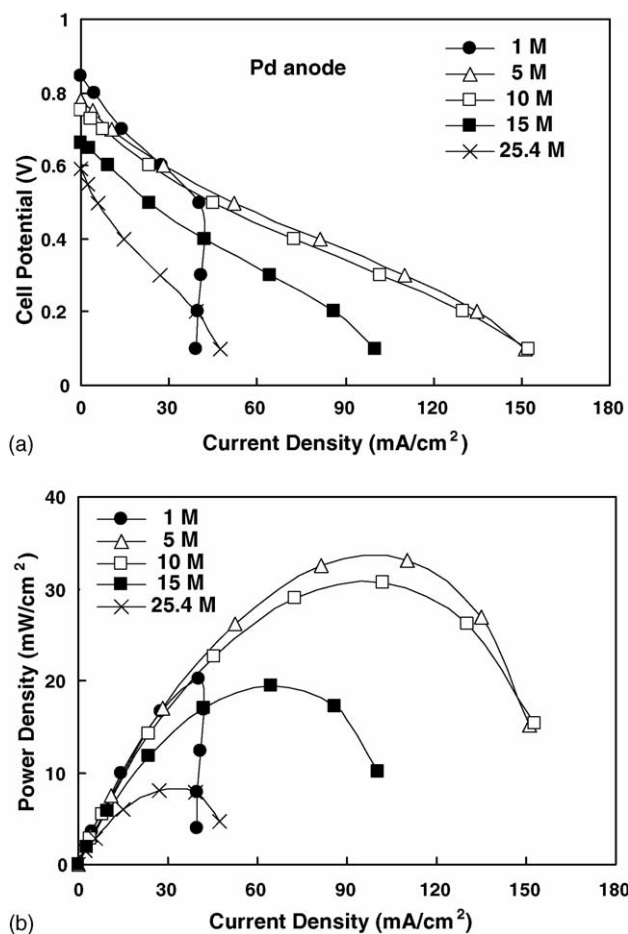


Fig. 4. Polarization (a) and power density (b) curves of a Si-DFAFC operating at room temperature with quiescent aqueous HCOOH solutions of different concentrations (1–25.4 M) on the anode (pure Pd) and a 10 sccm stream of  $\text{O}_2$  on the cathode (pure Pt).

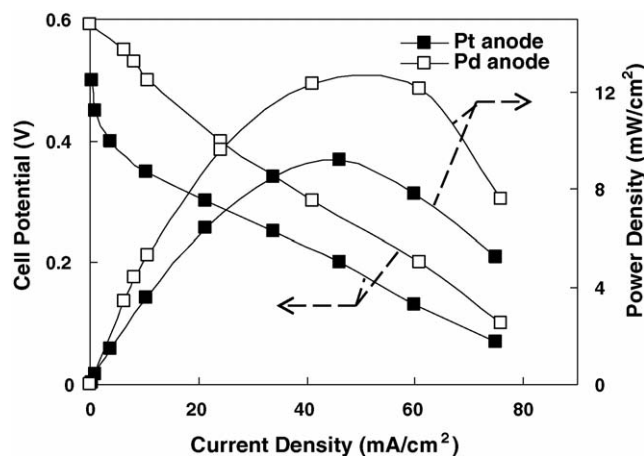


Fig. 5. Polarization and power density curves of a Si-DFAFC operated at room temperature using a quiescent aqueous 10 M HCOOH solution on the anode (pure Pt or pure Pd) and quiescent air on the cathode (pure Pt).

mance characteristics as other all-passive DMFCs and DFAFCs (Table 1), and, unlike many of those, the Si-DFAFCs studied here can be fabricated using processes that are post-CMOS compatible, thus enabling direct integration with MEMS-type applications.

#### 4. Conclusions

In this paper, we reported the performance of microfabricated Si-DFAFCs in which fuel delivery is passive: liquid formic acid fuel is in direct contact with the anode-side of the MEA, and the cathode is exposed to quiescent air, i.e., air-breathing. As expected, the maximum power density of these cells of  $30.7 \text{ mW cm}^{-2}$  as accomplished using a 10 sccm stream of oxygen at the cathode and a passive aqueous 10 M formic acid solution at the anode, is significantly higher than the maximum power density of  $12.3 \text{ mW cm}^{-2}$  for the same cell operated in an all-passive mode. Yet, eliminating the need for ancillary equipment such as air or fuel pumps and regulating electronics greatly reduce complexity and size (i.e., volume and weight) of a fuel cell-based microscale power source, thus increasing its specific energy, while reducing parasitic losses, cost, and potential for system failure. Compared to other all-passive DMFCs and DFAFCs (Table 1), the Si-DFAFCs reported here exhibit similar performance characteristics, yet the cells can be microfabricated using post-CMOS compatible processes and can thus be directly integrated with microscale applications such as MEMS sensors and actuators, simplifying overall application size, complexity, and manufacturing cost.

The Si-DFAFCs described here still offer opportunities for performance improvement. Firstly, integration of an ionomer such as Nafion within the catalyst structure at the anode side may improve proton conductivity from the sites of reaction on the catalyst structures to the Nafion membrane. For example, Missiroli et al. recently demonstrated improved methanol electro-oxidation when using Pt/Ru catalysts electrodeposited on Nafion-treated Carbon [46,47], a process that could also be implemented in the fabrication of the Si-DFAFCs studied here. Secondly, to avoid flooding of the cathode one could envision integration of a hydrophobic PTFE-treated carbon cloth, so water rising above the catalyst structures and thus creating a mass-transport barrier for incoming oxygen from air can be prevented.

#### Acknowledgements

The authors acknowledge generous support by the Defense Advanced Research Project Agency under U.S. Air Force Grant F33615-01-C-2172. All SEM work was conducted in the Center for Microanalysis of Materials, in the Frederick Seitz Material Research Laboratory, University of Illinois, which is partially supported by the U.S. Department of Energy under grant DEFC02-91-ER45439. Any opinions, findings, and conclusions or recommendations expressed in this publication are those of the authors and do not necessarily reflect the views of the Department of Energy, the U.S. Air Force, or the Defense Advanced Projects Research Agency.

#### References

- [1] J.D. Morse, A.F. Jankowski, R.T. Graff, J.P. Hayes, J. Vac. Sci. Technol. A 18 (4) (2000) 2003–2005.
- [2] S.J. Lee, A. Chang-Chien, S.W. Cha, R. O'Hayre, Y.I. Park, Y. Saito, F.B. Prinz, J. Power Sources 112 (2002) 410–418.
- [3] J. Yu, P. Cheng, Z. Ma, B. Yi, J. Power Sources 124 (2003) 40–46.
- [4] J. Yu, P. Cheng, Z. Ma, B. Yi, Electrochim. Acta 48 (2003) 1537–1541.
- [5] K. Shah, W.C. Shin, R.S. Besser, J. Power Sources 123 (2003) 172–181.
- [6] K. Shah, W.C. Shin, R.S. Besser, Sens. Actuators B 97 (2004) 157–167.
- [7] R. Hahn, S. Wagner, A. Schmitz, H. Reichl, J. Power Sources 131 (2004) 73–78.
- [8] Y. Yamazaki, Electrochim. Acta 50 (2004) 663–666.
- [9] S. Hsieh, C. Huang, J. Kno, H. Tsai, S. Yang, J. Solid State Electrochem. 9 (2005) 121–131.
- [10] S.H. Chan, N. Nguyen, Z. Xia, Z. Wu, J. Micromech. Microeng. 15 (2005) 231–236.
- [11] S.C. Kelley, G.A. Deluga, W.H. Smyrl, Electrochem. Solid State Lett. 3 (9) (2000) 407–409.
- [12] S.C. Kelly, G.A. Deluga, W.H. Smyrl, AIChE J. 48 (5) (2002) 1071–1082.
- [13] J.P. Meyers, H.L. Maynard, J. Power Sources 109 (2002) 76–88.
- [14] H.L. Maynard, J.P. Meyers, J. Vac. Sci. Technol. B 20 (4) (2002) 1287–1297.
- [15] T.J. Yen, N. Fang, X. Zhang, G.Q. Lu, C.Y. Wang, Appl. Phys. Lett. 83 (19) (2003) 4056–4058.
- [16] A. Blum, T. Duvdevani, M. Philosoph, N. Rudoy, E. Peled, J. Power Sources 117 (2003) 22–25.
- [17] G.Q. Lu, C.Y. Wang, T.J. Yen, X. Zhang, Electrochim. Acta 49 (2004) 821–828.
- [18] S. Motokawa, M. Mohamedi, T. Momma, S. Shoji, T. Osaka, Electrochem. Commun. 6 (2004) 562–565.
- [19] J. Li, C. Moore, P.A. Kohl, J. Power Sources 138 (2004) 211–215.
- [20] H.Y. Cha, H.G. Choi, J.D. Nam, Y. Lee, S.M. Cho, E.S. Lee, J.K. Lee, C.H. Chung, Electrochim. Acta 50 (2004) 795–799.
- [21] K. Wozniak, D. Johansson, M. Bring, A. Sanz-Velasco, P. Enoksson, J. Micromech. Microeng. 14 (2004) S59–S63.
- [22] J. Yeom, G.Z. Mozsgai, B.R. Flachsbart, E.R. Choban, A. Asthana, M.A. Shannon, P.J.A. Kenis, Sens. Actuators B 107 (2005) 882–891.
- [23] R.S. Jayashree, J.S. Spindelov, J. Yeom, C. Rastogi, M.A. Shannon, P.J.A. Kenis, Electrochim. Acta 50 (2005) 4674–4682.
- [24] J.L. Cohen, D.A. Westly, A. Pechenik, H.D. Abruna, J. Power Sources 139 (2005) 96–105.
- [25] J.L. Cohen, D.J. Volpe, D.A. Westly, A. Pechenik, H.D. Abruna, Langmuir 21 (2005) 2544–2550.
- [26] C.A. Rice, S. Ha, R.I. Masel, P. Waszczuk, A. Wieckowski, T. Barnard, J. Power Sources 111 (2002) 83–89.
- [27] S. Ha, C.A. Rice, R.I. Masel, A. Wieckowski, J. Power Sources 112 (2002) 655–659.
- [28] Y. Rhee, S. Ha, R.I. Masel, J. Power Sources 117 (2003) 35–38.
- [29] Y. Zhu, S. Ha, R.I. Masel, J. Power Sources 130 (2004) 8–14.
- [30] S. Ha, R. Larsen, Y. Zhu, R.I. Masel, Fuel Cells 4 (2004) 337–343.
- [31] S. Ha, R. Larsen, R.I. Masel, J. Power Sources 144 (2005) 28–34.
- [32] A. Heinzl, C. Hebling, M. Müller, M. Zedda, C. Müller, J. Power Sources 105 (2002) 250–255.
- [33] H. Chang, J.R. Kim, J.H. Cho, H.K. Kim, K.H. Choi, Solid State Ionics 148 (2002) 601–606.
- [34] J. Han, E.S. Park, J. Power Sources 112 (2002) 477–483.
- [35] C.Y. Chen, P. Yang, J. Power Sources 123 (2003) 37–42.
- [36] A. Schmitz, M. Tranitz, S. Wagner, R. Hahn, C. Hebling, J. Power Sources 118 (2003) 162–171.
- [37] Z. Guo, Y. Cao, J. Power Sources 132 (2004) 86–91.
- [38] T. Shimizu, T. Momma, M. Mohamedi, T. Osaka, S. Sarangapani, J. Power Sources 137 (2004) 277–283.
- [39] D.J. Kim, E.A. Cho, S.A. Hong, I.H. Oh, H.Y. Ha, J. Power Sources 130 (2004) 172–177.

- [40] B.K. Kho, I.H. Oh, S.A. Hong, H.Y. Ha, *Electrochim. Acta* 50 (2004) 781–785.
- [41] B.K. Kho, B. Bae, M.A. Schibioh, J. Lee, H.Y. Ha, *J. Power Sources* 142 (2005) 50–55.
- [42] J.G. Liu, T.S. Zhao, R. Chen, C.W. Wong, *Electrochem. Commun.* 7 (2005) 288–294.
- [43] S. Ha, B. Adams, R.I. Masek, *J. Power Sources* 128 (2004) 119–124.
- [44] C. Rice, S. Ha, R.I. Masek, A. Wieckowski, *J. Power Sources* 115 (2003) 229–235.
- [45] G.-Q. Lu, A. Crown, A. Wieckowski, *J. Phys. Chem. B* 103 (1999) 9700–9711.
- [46] M. Mastragostino, A. Missiroli, F. Soavi, *J. Electrochem. Soc.* 151 (2004) A1919–A1924.
- [47] A. Missiroli, F. Soavi, M. Mastragostino, *Electrochem. Solid State Lett.* 8 (2005) A110–A114.